Journal of Energy Storage 63 (2023) 107105

Contents lists available at ScienceDirect

Journal of Energy Storage

journal homepage: www.elsevier.com/locate/est

Research papers

Plasmonic based fibre optic detection and electrochemical identification of phase transitions in NMC111/graphite lithium-ion pouch cells

Christopher Gardner [a,*], Elin Langhammer [b], Alexander J. Roberts [a], Tazdin Amietszajew [a]

[a] Coventry University, Coventry CV1 5FB, UK
[b] Insplorion AB, Arvid Wallgrens backe 20, 413 46 Göteborg, Sweden

ARTICLE INFO

Keywords:
Plasmonic sensing
Fibre optic
Diagnostics
Li-ion battery
Phase transitions
Incremental capacity analysis

ABSTRACT

This work expands on the use of plasmonic based fibre optic sensors as an in-situ diagnostic sensor inside Li-ion NMC111 pouch cells, with the sensors positioned adjacent to both the negative and the positive electrodes. Via incremental capacity analysis (IC) of the full cell, of individual electrodes utilising a reference electrode and cyclic voltammetry (CV) techniques, the electrode state changes are identified and the relationship to the plasmonic optical signal is observed. We report identification of electrode phase transitions via electrochemical methods and the corresponding response of in-situ plasmonic based fibre optic sensors.

1. Introduction

The growth of the battery market is well documented, driven by numerous industries including automotive, grid storage and portable electronic devices, industries which predominantly utilise Li-ion batteries [1–3]. Within the category of li-ion cells, layered intercalation compounds (LIC) play a significant role due to the relatively high volumetric and gravimetric energy densities, high operating voltages and good electric conductivity. NMC type (such as $LiN_{1/3}M_{1/3}C_{1/3}O_2$ – NMC) is a particularly utilised LIC chemistry in electric vehicles (EV's) and energy storage, other LIC chemistries are also utilised such as NCA (i.e. $LiNi_{0.85}Co_{0.1}Al_{0.05}O_2$) which is found in EV's and energy storage and LCO (i.e. $LiCoO_2$) which is common in power electronics [1,4]. The phospho-olivine chemistry LFP (LiFePO4) is also an increasingly common chemistry used in EV's, with benefits including more abundant and affordable materials, relatively flat voltage charge profile and improved safety [5].

With the growing uptake and complexity of Li-ion battery systems, superior diagnostics can have a range of benefits including research insights, improved safety, battery use optimisation and supporting applications such as second life uses and the 'battery passport' concept [6]. Fibre optic based sensing techniques have demonstrated significant value as in-situ and in-operando battery diagnostic techniques and continue to be an area of significant research and development [7,8]. Fibre Bragg Gratings (FBG's) and Tilted Fibre Bragg Gratings (TFBG's) are utilised for temperature and strain measurements [9–12], identifying phase changes and diffusion rates through strain measurements [13,14], SEI layer formation detection [15] and even State of Charge estimation via strain measurement [16]. Fibre optic evanescent wave sensor (FOEWS) techniques, also known as attenuated total reflection (ATR), have demonstrated optical signal correlation to cell charge and discharge [17–19] and graphite lithiation [20]. FOEWS and Fourier-transform infrared spectroscopy (FTIR) techniques have also demonstrated lithium ion concentration measurements [21]. Additionally, electrode strain measurements have been obtained via fibre optic sensors with Rayleigh scattering [22].

The use of plasmonic based fibre optic sensors has recently been demonstrated in li-ion pouch cells [3] and to measure lithium ion concentration in aqueous battery electrolyte [23]. In this study, we demonstrate the potential value of this diagnostic technique for cell characterisation, by identification of phase changes in Li-ion NMC111 cells during cycling utilising the plasmonic fibre optical signal. NMC111 is a transition metal oxide layered intercalation cathode that stores lithium ions between the lattice layers [24,25]. During deintercalation of lithium ions, when charging the cell, the charge compensation mechanism is understood to be oxidation of the Ni^{2+} ions to Ni^{3+} and Ni^{4+} [26–28]. As the transition metal elements are oxidised during cell charging the Jahn-Teller effect leads to distortion of the octahedral structures within the lattice [29]. The graphite anode also undergoes structural changes during charge as lithium ions intercalates into it, from unlithiated carbon through to fully lithiated LiC_6 [30–35].

This paper details the use of plasmonic based fibre optic sensors and

* Corresponding author.
E-mail address: gardne62@uni.coventry.ac.uk (C. Gardner).

https://doi.org/10.1016/j.est.2023.107105
Received 3 November 2022; Received in revised form 16 January 2023; Accepted 8 March 2023
Available online 15 March 2023

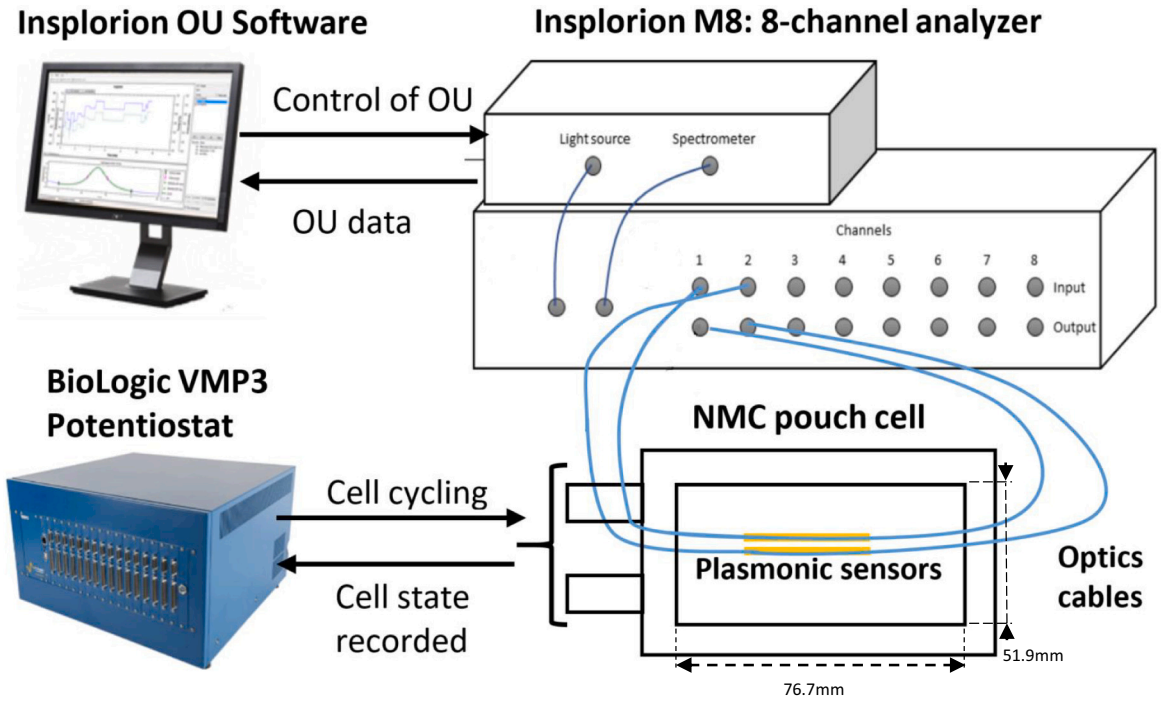

Fig. 1. Optical unit, potentiostat and cell with sensors schematic sketch (including cell dimensions, not to scale).

the signals obtained from both the cathode and anode in li-ion NMC pouch cells. Cyclic voltammetry and slow galvanostatic cycling followed by incremental capacity (IC) analysis is utilised to identify phase transitions in the cell. A lithium reference electrode is also utilised to carry out IC analysis on the cathode and anode separately. Analysis of the simultaneously collected optical data shows corresponding detection of the phase transitions in the cell via peaks in the differentiated optical signal. These results can potentially provide further insight into NMC111 phase transition events and further demonstrate the potential of plasmonic based fibre optic sensing to identify processes occurring within lithium-ion cells.

2. Methodology

The cells used for this experimentation are multi-layer pouch cells weighing 29.4 g ± 0.2 g when dry (no electrolyte), with lithium nickel manganese cobalt oxide ($LiNi_{1/3}Mn_{1/3}Co_{1/3}O_2$, NMC 111) cathode and graphite anode at a loading of 2 mAh cm^{-2}. The cell dimensions are shown in Fig. 1. The cells are filled with 1 M LiPF6 in EC/EMC (3/7 *v/v*) electrolyte and have a capacity of 1400 mAh. All cells were formed with two cycles of constant current charge at C/20 to 4.2 V, with constant voltage charge to a current limit of C/100 and subsequent discharge to 2.5 V at C/20.

In the case of the cells with fibre optic sensors, two plasmonic based fibre sensors are placed in the cell prior to the initial pouch sealing. One sensor is placed adjacent to a cathode and one sensor adjacent to an anode, allowing simultaneous measurement of both electrodes. The cell is made up of 21 electrode layers (11 anode and 10 cathode), the sensors are placed adjacent to the 3rd electrode (anode) and 4th electrode (cathode) from the edge. Further details around the cell manufacturing process can be found in a previous publication [3]. A cell with a lithium metal reference electrode is also prepared to allow separate cathode and anode voltage measurements, which was then cycled according to the same galvanostatic cycling conditions as the other cells to allow a direct comparison of the results and IC analysis of the individual electrodes as well as the full cell.

In order to analyse cell phase changes two electrochemical analysis techniques have been utilised, incremental capacity and cyclic voltammetry. Incremental capacity analysis, also known as differential capacity analysis, allows identification of phase transitions via peaks in the plot which correspond to voltage plateaus in the charge voltage profile [36]. Cyclic voltammetry displays peaks during electrode oxidation or reduction processes [37,38]. The cycling regimes of the test are detailed in Table 1.

Table 1
Cell test programs.

Cells tested	Test type	Cycle steps	Current/ voltage input	Until limit
Reference cells, cells with fibre sensors and cell with reference electrode	Incremental capacity analysis	Constant current (CC) charge	70 mA (capacity (C)/20)	4.2 V
		Constant voltage (CV) charge	4.2 V, variable current	First of C/100 or 4 h.
		Constant current discharge	70 mA (C/ 20)	2.5 V
Cell with fibre sensors on anode and cathode	Cyclic voltammetry	Voltage sweep	0.05 mVs^{-1}	4.2 V
		Voltage sweep	0.05 mVs^{-1}	2.5 V

The optical measurements in the experimentation are carried out utilising plasmonic sensor fibres (silica fibres with gold coated sensing region, protected by polymer coatings) and an M8: 8 Channel Analyser optical unit transmitter and receiver device, including software for control of the optical unit settings and data capture, provided by Insplorion AB (Göteborg, Sweden). The plasmonic fibre sensor function couples the evanescent wave generated by the internally reflected light in the fibre with the surface of the gold coating to generate a surface plasmon wave (SPW) of oscillating electrons along the surface of the gold film. The light signal in the optical fibre is attenuated at the frequency of the surface plasmon wave, while a change in the refractive index of the adjacent analyte changes the resonant frequency of the SPW

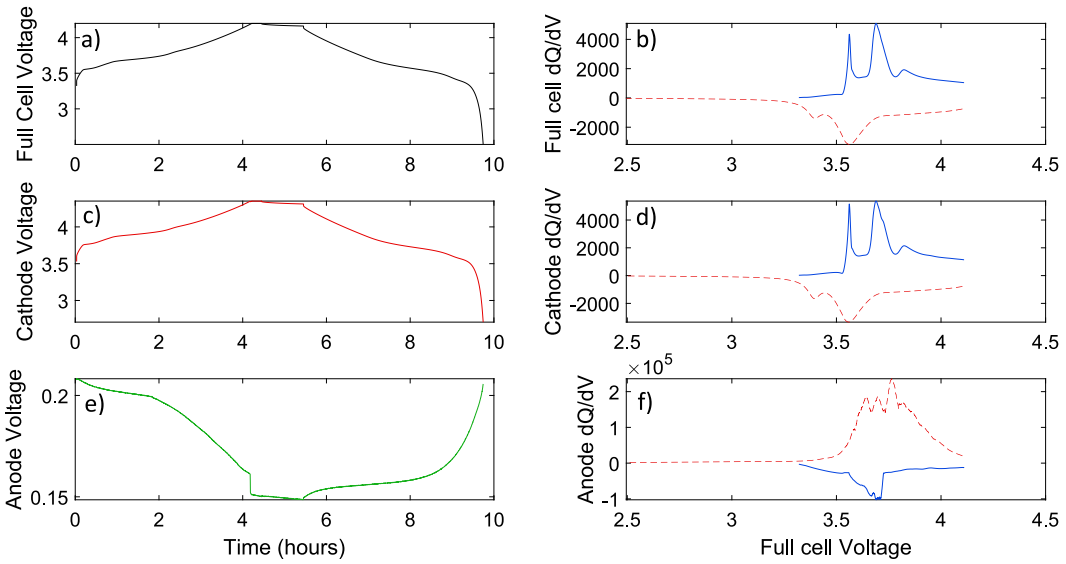

Fig. 2. Time-Voltage (T-V) and IC plots (solid blue line is charge, dotted red line is discharge) on NMC111 cell with graphite anode and Lithium reference electrode cycles at 240 mA (C/5); a) Full T-V plot, b) Full cell IC plot, c) Cathode Time-Voltage plot, d) Cathode IC Plot, e) Anode T-V Plot, f) Anode IC Plot. (For interpretation of the references to color in this figure legend, the reader is referred to the web version of this article.)

and subsequent frequency of light signal attenuation; in this way a change in analyte refractive index leads to a change in fibre light signal attenuation which can be measured from the output of the light signal passing through the fibre. The plasmonic sensor has a sensing depth of approximately 1000 nm, with exponentially decreasing sensitivity throughout this sensing region. Further details around the sensor design and the light interrogation mechanisms at work can be found in a previous publication and other literature [3,39].

The integration time and number of measurement averages taken per measurement are selected to ensure an accurate reading without saturating the optical receiver. The sampling rate was set at 30s intervals for this experimentation, to ensure sufficient time resolution. The fibre optic cables (Thorlabs) and 'pigtails' (SQS) connecting the sensor to the optical unit have low hydroxyl multimode Ø105 μm silica fibre cores. A sketch of the equipment setup can be seen in Fig. 1. The cells with fibre sensors are placed in a temperature controlled oven (Binder GmbH, Tuttlingen, Germany), maintained at 25 °C for these experiments. Here it is also noted that previous studies indicate the presence of the fibre sensor has a negligible impact on the cell performance [3].

The data has been processed in Matlab 2021a for data analysis and graph plotting. In the IC plots in Fig. 2, the constant voltage and rest steps at the extremes of the cycles have been excluded. The optical signal recorded is the light intensity at the 725 nm wavelength, previously identified as the most attuned to the analyte change of interest [3]. In the optical signal differential analysis a Savitzky-Golay filter has been used to remove noise from the signal and help to isolate the large differential responses.

3. Results and discussion

Full cell and individual electrode voltage profiles for a full charge and discharge cycle are shown in Fig. 2. The associated IC plots are also shown, for which the total cell charge has been differentiated with respect to the respective voltages. The CV and rest portions of the cycle have been trimmed from the IC plots, and a Savitzky-Golay filter has been applied to smooth the signal without distorting the profile.

The full cell IC plot in Fig. 2b has two clear peaks on the charge and the discharge cycles, indicating two reversible phase transitions. This profile is closely matched by that of the cathode IC plot in Fig. 2d, indicating that the phase changes are being measured at the cathode and that the cathode is the dominant influencing electrode on overall cell

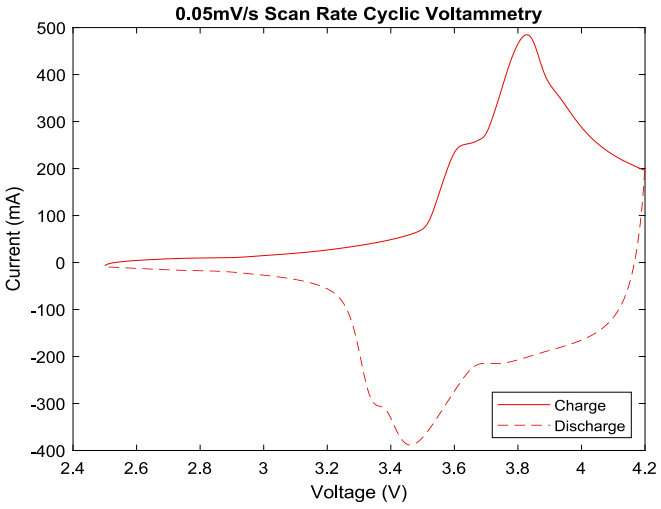

Fig. 3. Cyclic voltammetry plot of NMC111 cell with graphite electrode, scan rate of 0.05mVs^{-1}.

voltage change during cycling. A third smaller peak can be seen on the charge cycle but not the discharge cycle, this suggests an irreversible process and has in other studies been attributed to SEI layer formation [40,41]. The cyclic voltammetry plot shown in Fig. 3 similarly indicates the presence of two reversible phase transition events via two major peaks, but does not detect the SEI layer formation as the IC analysis does.

Full cell IC plots obtained here match existing literature on cells with NMC111 cathodes and graphite electrodes, with the same distinctive double peak on the charge and discharge cycles [40,42]. In some literature the first peak is identified as lithium intercalation into the graphite anode ($C_6 \rightarrow LiC_x$) and the second peak as the phase transition from a hexagonal to a monoclinic (H1 → M) lattice of the NMC [40–42]. This identification is supported further by studies on NMC111 vs lithium half cells in which only one clear CV peak [43–45] was identified. However, the IC plots shown by Noh et al. [44] and diffusion coefficient during cycling as reported by Fröhlich et al. [43] do indicate existence of two peaks even in the case of such half cells, with a smaller shoulder peak within a larger second peak. Furthermore, theoretical studies have

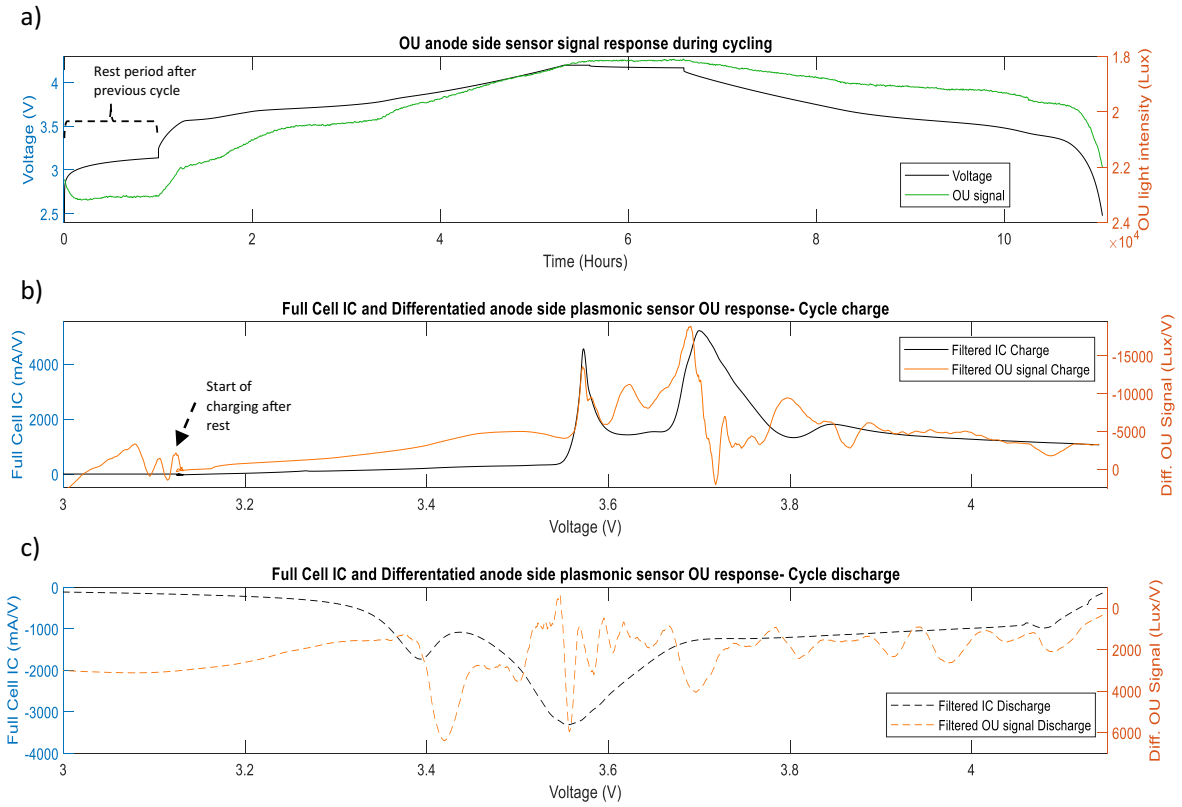

Fig. 4. a) Cell voltage and anode side sensor optical response (lux) over time, b) Full cell IC plot and differentiated optical signal plot during charge, c) Full cell IC plot and differentiated optical signal plot during discharge.

reported Ni^{2+}/Ni^{3+} and Ni^{3+}/Ni^{4+} charge compensation mechanisms as lithium leaves the metal oxide structure during charging [27,28,46] (with other models suggesting cobalt oxidation could play a role [46]), while material analysis studies also report the presence of Ni^{3+} and Ni^{4+} ions during NMC111 charge [26], significantly two stages of oxidation also imply two phase change steps.

The observation of the cathode IC in this paper (Fig. 2d) coupled with the above discussed literature suggest that the two measured peaks could represent a two stage process of phase transition in the NMC through the $Ni^{2+} \rightarrow Ni^{3+}$ and $Ni^{3+} \rightarrow Ni^{4+}$ oxidation steps. Factors that could influence this process and lead to variation in reported literature observations include rate of charge, material of counter electrode and particle size of the working electrode. The reference electrode data identifies both of these peaks as predominant on the cathode IC plot, as shown in Fig. 2d, which can be expected due to the greater contribution of the cathode to the cell voltage change. This could indicate that both of the significant and reversible phase transition events identified on the full cell IC plot (Fig. 2b) are due to cathodic phase transition events.

The anode IC plot in Fig. 2f indicates multiple peaks, in line with lithium intercalation stages at the graphite electrode. There are four distinct peak features, which is consistent with the literature listing broader major LiC_{12} and LiC_6 intercalation compounds during cell charge and within that five phases and four transition events. Studies have shown that the graphite phase transition process is not symmetrically reversible [30–35], which is also reflected in the asymmetric IC curves for the anode from charge to discharge in Fig. 2f.

Considering the measured optical data, both the anode and cathode side sensors seem to respond in to the phase transition events identified by the two large full cell IC peaks, as shown in Figs. 4 and 5; an interesting finding for this diagnostic method as it showcases capability to detect this internal cell event in real time. There seems to be a clear optical response when the cell charging starts, at the full cell phase transition IC peaks and the SEI layer formation peak. While these responses are visible there are also other smaller features within the optical signal, which could correlate to other cell events such as anodic phase transitions (which can be seen in the Fig. 2f reference electrode data but are not visible across the full cell IC plot in Fig. 2b), micro events in the localised region of the sensor and some noise factor induced by other variables such as strain, temperature and vibration.

Previous studies have hypothesised that the plasmonic based fibre optic sensors are measuring lithium ion concentration at the surface of the adjacent electrode [3]. A study which uses plasmonic sensing to measure the ion concentration in an aqueous battery electrolyte supports the proposal that the sensors are sensitive to lithium ion concentration in batteries [23]. ATR has also been demonstrated to measure concentration changes in a liquid electrolyte in a lithium metal anode half-cell [21]. As noted previously, studies have observed that the lithium ion diffusion coefficient of the NMC metal oxide electrode changes during phase transition events [43]. The proposed hypothesis is therefore that the change in diffusion coefficient results in an acceleration/deceleration of the lithium ions concentration change adjacent to the electrode surface, which is then detected by the plasmonic based fibre optic sensor. The sensing depth of the plasmonic sensor is such that the measured region of the electrode should primarily be the boundary layer in this case, implying that diffusion of lithium within the solid phase is the rate determining step.

As well as lithium ion concentration, other variables such as strain and temperature also have to be considered. In terms of strain, the relationship between cell charge and electrode expansion is well documented, explained by intercalation of lithium ions and corresponding changes in the electrode lattice structures [14]. Numerous fibre optic based sensor studies, utilising techniques such as FBG's [13,16,47,48] and Rayleigh Scattering [49] have demonstrated the relationship between cell cycling and strain. In this case the fibre is not mechanically adhered to the electrode so is unlikely to be responding to direct strain. Also it has been demonstrated that optical signal responds most strongly

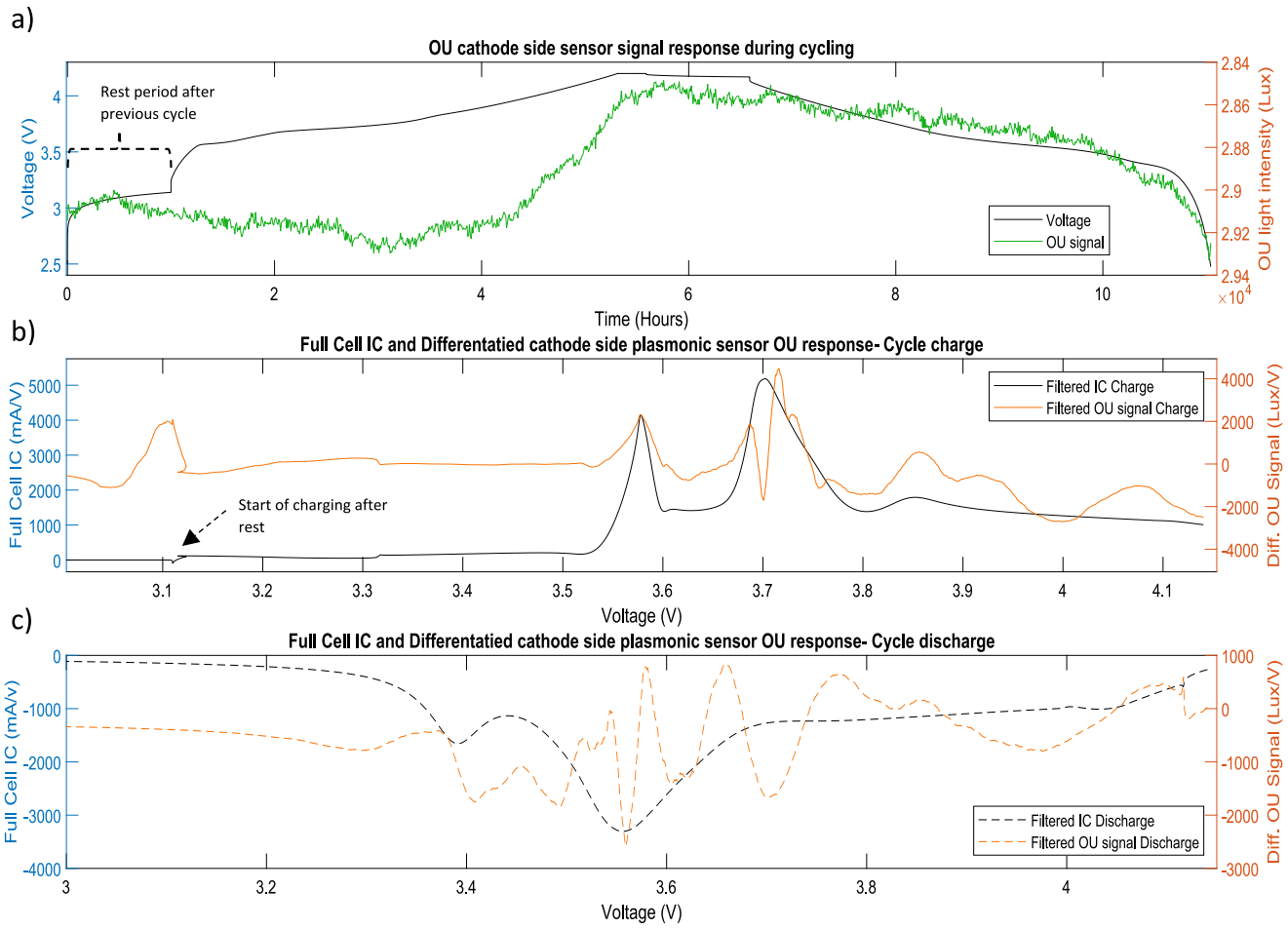

Fig. 5. a) Cell voltage and cathode side sensor optical response (lux) over time, b) Full cell IC plot and differentiated optical signal plot during charge, c) Full cell IC plot and differentiated optical signal plot during discharge.

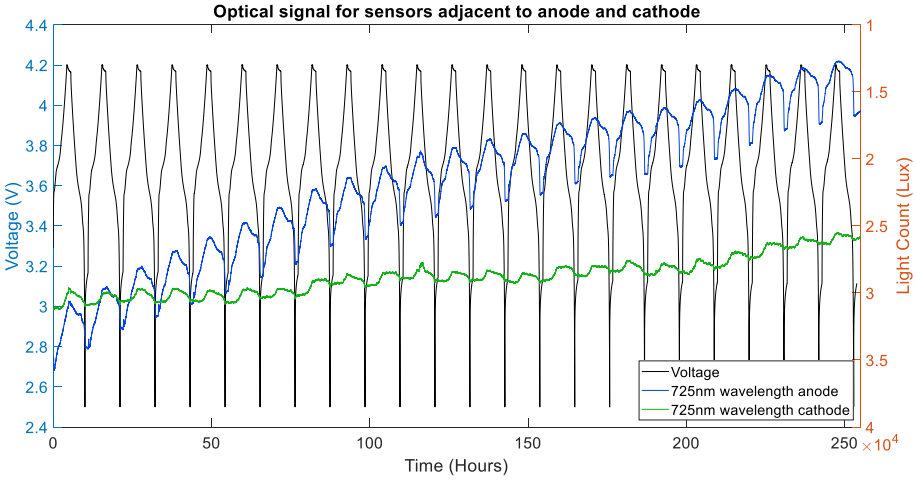

Fig. 6. 23 cycles of NMC111 cell with plasmonic fibre sensors adjacent to an anode and cathode electrode-graph shows voltage and optical signal of sensor at anode and cathode over time.

to cathodic phase transition, if anode expansion where being measured then there should be a stronger response to anodic events, for example anode expansion during charging has been measured at 6.1 % by Stage 2 (LiC_{12}) and 13.2 % by stage 1 (LiC_6) [35,50], while NMC111 cathode volume change during cycling is typically ~1 % [51]. Temperature effects are also minimal, due to the slow rate of cycling and controlled oven temperature. As such it can be assumed strain and temperature are not dominant measurands.

Fig. 6 shows the anode sensor and cathode sensor optical signal strength at the 725 nm wavelength during cycling. Both signals demonstrate a qualitative correlation with cell voltage state during charge and discharge. Notable differences include the anode side optical

signal more closely following the profile of the voltage, while also exhibiting greater light extinction over time. Greater anode side extinction could be explained by SEI layer growth, or the fibre protective coating failing between the sensor and anode causing lithiation of the gold sensing region or silica fibre at low electrode voltages. The fact the sensor signal extinction is not as significant on the cathode side indicates that it is not just a consequence of sensor integrity deterioration due to the corrosive environment of the cell.

4. Conclusions

In this study we demonstrate for the first time the detection of lithium-ion cell phase transitions via in-situ plasmonic based fibre optic sensors. The optical sensors are successfully implemented inside multi-layered NMC and graphite pouch cells, with sensors adjacent to both the anode and cathode providing correlating data.

Electrode phase transitions identified by the optical cell data are confirmed across the full cell and on individual electrodes via IC methods and a reference electrode. The IC data obtained on individual electrode is used to support the identification of the observed phenomena and suggests both full cell IC peaks could be cathodic events. The optical signal data correlation to the phase transition events is hypothesised to be due to the secondary effect of the change in the rate of lithium diffusion, leading to lithium ion concentration rate changes at the electrode surface that is detected by the sensor.

This work further demonstrates the potential of plasmonic based fibre optic sensors as an in-situ battery diagnostic technique capable of detecting internal cell processes in real time. Systemic testing should be carried out to prove the hypothesis that the plasmonic sensor is sensitive to changes in the electrode boundary layer. Additionally further work can continue to build on the use of this sensor, including the response to failure modes such as lithium plating, behaviour in more varied cell cycling profiles, multi-sensored cells to deconvolute temperature and strain effects and experimentation and analysis to further explore and quantify the relationship to State of Charge and State of Health.

Declaration of competing interest

Christopher Gardner reports financial support and equipment, drugs, or supplies were provided by Insplorion AB. Elin Langhammer reports a relationship with Insplorion AB that includes: board membership and employment.

Data availability

The data generated and analysed during this study is available on request, although some restricitons may apply to any details our industrial partners consider commercially confidential.

References

[1] I. Tsiropoulos, D. Tarvydas, N. Lebedeva, Li-ion Batteries for Mobility and Stationary Storage Applications, 2018, https://doi.org/10.2760/87175.

[2] P. Harrop, X. He, D. Gatti, Distributed generation: off-grid zero-emission kW-MW 2020–2040, IDTechEx (2020). https://www.idtechex.com/en/research-report/distributed-generation-off-grid-zero-emission-kw-mw-2020-2040/730 (accessed August 17, 2020).

[3] C. Gardner, E. Langhammer, W. Du, D.J.L. Brett, P.R. Shearing, A.J. Roberts, T. Amietszajew, In-situ Li-ion pouch cell diagnostics utilising plasmonic based optical fibre sensors, Sensors. 22 (2022) 738, https://doi.org/10.3390/s22030738.

[4] P. Jehnichen, K. Wedlich, C. Korte, Degradation of high-voltage cathodes for advanced lithium-ion batteries–differential capacity study on differently balanced cells, Sci. Technol. Adv. Mater. 20 (2019) 1–9, https://doi.org/10.1080/14686996.2018.1550625.

[5] C.P. Aiken, E.R. Logan, H. Hebecker, J.M. Oxner, J. Harlow, M. Metzger, J.R. Dahn, Li[Ni0.5Mn0.3Co0.2]O2 as a superior alternative to LiFePO4 for long-lived low voltage Li-ion cells, in: ECS Meet. Abstr. MA2021-02, 2021, p. 1893, https://doi.org/10.1149/ma2021-0251893mtgabs.

[6] K. Berger, J.P. Schöggl, R.J. Baumgartner, Digital battery passports to enable circular and sustainable value chains: conceptualization and use cases, J. Clean. Prod. 353 (2022), 131492, https://doi.org/10.1016/j.jclepro.2022.131492.

[7] J. Huang, S.T. Boles, J.M. Tarascon, Sensing as the key to battery lifetime and sustainability, Nat. Sustain. 5 (2022) 194–204, https://doi.org/10.1038/s41893-022-00859-y.

[8] Y.-D. Su, Y. Preger, H. Burroughs, C. Sun, P. Ohodnicki, Fiber optic sensing technologies for battery management systems and energy storage applications, Sensors. 21 (2021) 1397, https://doi.org/10.3390/s21041397.

[9] T. Amietszajew, E. McTurk, J. Fleming, R. Bhagat, Understanding the limits of rapid charging using instrumented commercial 18650 high-energy Li-ion cells, Electrochim. Acta 263 (2018) 346–352, https://doi.org/10.1016/j.electacta.2018.01.076.

[10] M. Nascimento, S. Novais, M.S. Ding, M.S. Ferreira, S. Koch, S. Passerini, J.L. Pinto, Internal strain and temperature discrimination with optical fiber hybrid sensors in Li-ion batteries, J. Power Sources 410–411 (2019) 1–9, https://doi.org/10.1016/j.jpowsour.2018.10.096.

[11] M. Nascimento, M.S. Ferreira, J.L. Pinto, Temperature fiber sensing of Li-ion batteries under different environmental and operating conditions, Appl. Therm. Eng. 149 (2019) 1236–1243, https://doi.org/10.1016/j.applthermaleng.2018.12.135.

[12] A. Nedjalkov, J. Meyer, A. Gräfenstein, B. Schramm, M. Angelmahr, J. Schwenzel, W. Schade, Refractive index measurement of lithium ion battery electrolyte with etched surface cladding waveguide Bragg gratings and cell electrode state monitoring by optical strain sensors, Batteries. 5 (2019) 30, https://doi.org/10.3390/batteries5010030.

[13] L.W. Sommer, P. Kiesel, A. Ganguli, A. Lochbaum, B. Saha, J. Schwartz, C.J. Bae, M. Alamgir, A. Raghavan, Fast and slow ion diffusion processes in lithium ion pouch cells during cycling observed with fiber optic strain sensors, J. Power Sources 296 (2015) 46–52, https://doi.org/10.1016/j.jpowsour.2015.07.025.

[14] L.W. Sommer, A. Raghavan, P. Kiesel, B. Saha, J. Schwartz, A. Lochbaum, A. Ganguli, C.-J. Bae, M. Alamgir, Monitoring of intercalation stages in lithium-ion cells over charge-discharge cycles with fiber optic sensors, J. Electrochem. Soc. 162 (2015) A2664–A2669, https://doi.org/10.1149/2.0361514jes.

[15] J. Huang, L. Albero Blanquer, J. Bonefacino, E.R. Logan, D. Alves Dalla Corte, C. Delacourt, B.M. Gallant, S.T. Boles, J.R. Dahn, H.Y. Tam, J.M. Tarascon, Operando decoding of chemical and thermal events in commercial Na(Li)-ion cells via optical sensors, Nat. Energy (2020) 1–10, https://doi.org/10.1038/s41560-020-0665-y.

[16] A. Ganguli, B. Saha, A. Raghavan, P. Kiesel, K. Arakaki, A. Schuh, J. Schwartz, A. Hegyi, L.W. Sommer, A. Lochbaum, S. Sahu, M. Alamgir, Embedded fiber-optic sensing for accurate internal monitoring of cell state in advanced battery management systems part 2: internal cell signals and utility for state estimation, J. Power Sources 341 (2017) 474–482, https://doi.org/10.1016/j.jpowsour.2016.11.103.

[17] J. Hedman, D. Nilebo, E. Larsson Langhammer, F. Björefors, Fibre optic sensor for characterisation of lithium-ion batteries, ChemSusChem. 13 (2020) 5731–5739, https://doi.org/10.1002/cssc.202001709.

[18] J. Hedman, F. Björefors, Fiber optic monitoring of composite lithium iron phosphate cathodes in pouch cell batteries, ACS Appl. Energy Mater. 5 (2022) 870–881, https://doi.org/10.1021/acsaem.1c03304.

[19] A. Ghannoum, P. Nieva, A. Yu, A. Khajepour, Development of embedded fiber-optic evanescent wave sensors for optical characterization of graphite anodes in lithium-ion batteries, ACS Appl. Mater. Interfaces 9 (2017) 41284–41290, https://doi.org/10.1021/acsami.7b13464.

[20] A.R. Ghannoum, P. Nieva, Graphite lithiation and capacity fade monitoring of lithium ion batteries using optical fibers, J. Energy Storage. 28 (2020), 101233, https://doi.org/10.1016/j.est.2020.101233.

[21] L. Meyer, D. Curran, R. Brow, S. Santhanagopalan, J. Porter, Operando measurements of electrolyte Li-ion concentration during fast charging with FTIR/ATR, J. Electrochem. Soc. 168 (2021), 090502, https://doi.org/10.1149/1945-7111/ac1d7a.

[22] E. Vergori, Y. Yu, Monitoring of Li-ion Cells With Distributed Fibre Optic Sensors, in: Procedia Struct. Integr., Elsevier B.V., 2019, pp. 233–239, https://doi.org/10.1016/j.prostr.2020.02.020.

[23] R. Wang, H. Zhang, Q. Liu, F. Liu, X. Han, X. Liu, K. Li, G. Xiao, J. Albert, X. Lu, T. Guo, Operando monitoring of ion activities in aqueous batteries with plasmonic fiber-optic sensors, Nat. Commun. 13 (2022) 547, https://doi.org/10.1038/s41467-022-28267-y.

[24] N. Nitta, F. Wu, J.T. Lee, G. Yushin, Li-ion battery materials: present and future, Mater. Today 18 (2015) 252–264, https://doi.org/10.1016/J.MATTOD.2014.10.040.

[25] K. Fröhlich, I. Abrahams, M. Jahn, Determining phase transitions of layered oxides via electrochemical and crystallographic analysis, Sci. Technol. Adv. Mater. 21 (2020) 653–660, https://doi.org/10.1080/14686996.2020.1814116/SUPPL_FILE/TSTA_A_1814116_SM7890.PDF.

[26] W.S. Yoon, M. Balasubramanian, K.Y. Chung, X.Q. Yang, J. McBreen, C.P. Grey, D. A. Fischer, Investigation of the charge compensation mechanism on the electrochemically Li-ion deintercalated Li1-xCo1/3Ni1/3Mn 1/3O2 electrode system by combination of soft and hard X-ray absorption spectroscopy, J. Am. Chem. Soc. 127 (2005) 17479–17487, https://doi.org/10.1021/ja0530568.

[27] Y. Koyama, I. Tanaka, H. Adachi, Y. Makimura, T. Ohzuku, Crystal and electronic structures of superstructural Li1-x[Co1/3Ni1/3Mn1/3]O2 ($0 \leq x \leq 1$), in, J. Power Sources (2003) 644–648, https://doi.org/10.1016/S0378-7753(03)00194-0.

[28] B.J. Hwang, Y.W. Tsai, D. Carlier, G. Ceder, A combined computational/experimental study on LiNi1/3Co1/3Mn1/3O2, Chem. Mater. 15 (2003) 3676–3682, https://doi.org/10.1021/cm030299v.
[29] H. Sun, K. Zhao, Electronic structure and comparative properties of LiNi x Mn y Co z O 2 cathode materials, J. Phys. Chem. C 121 (2017) 6002–6010, https://doi.org/10.1021/acs.jpcc.7b00810.
[30] Y. Guo, R.B. Smith, Z. Yu, D.K. Efetov, J. Wang, P. Kim, M.Z. Bazant, L.E. Brus, Li intercalation into graphite: direct optical imaging and Cahn-Hilliard reaction dynamics, J. Phys. Chem. Lett. 7 (2016) 2151–2156, https://doi.org/10.1021/acs.jpclett.6b00625.
[31] W. Li, J. Zhu, Experimental study on lithium ion diffusion of graphite anode based on in-situ optics, IOSR J. Eng. 09 (2019) 62–65.
[32] P. Maire, A. Evans, H. Kaiser, W. Scheifele, P. Novák, Colorimetric determination of lithium content in electrodes of lithium-ion batteries, J. Electrochem. Soc. 155 (2008) A862, https://doi.org/10.1149/1.2979696.
[33] J.J. Lodico, C.H. Lai, M. Woodall, H.L. Chan, E. Garcia, W.A. Hubbard, B. Dunn, B. C. Regan, Irreversibility at macromolecular scales in the flake graphite of the lithium-ion battery anode, J. Power Sources 436 (2019), 226841, https://doi.org/10.1016/j.jpowsour.2019.226841.
[34] S. Taminato, M. Yonemura, S. Shiotani, T. Kamiyama, S. Torii, M. Nagao, Y. Ishikawa, K. Mori, T. Fukunaga, Y. Onodera, T. Naka, M. Morishima, Y. Ukyo, D. S. Adipranoto, H. Arai, Y. Uchimoto, Z. Ogumi, K. Suzuki, M. Hirayama, R. Kanno, Real-time observations of lithium battery reactions - operando neutron diffraction analysis during practical operation, Sci. Rep. 6 (2016) 1–12, https://doi.org/10.1038/srep28843.
[35] S. Schweidler, L. De Biasi, A. Schiele, P. Hartmann, T. Brezesinski, J. Janek, Volume changes of graphite anodes revisited: a combined operando X-ray diffraction and in situ pressure analysis study, J. Phys. Chem. C 122 (2018) 8829–8835, https://doi.org/10.1021/acs.jpcc.8b01873.
[36] A. Fly, R. Chen, Rate dependency of incremental capacity analysis (dQ/dV) as a diagnostic tool for lithium-ion batteries, J. Energy Storage. 29 (2020), 101329, https://doi.org/10.1016/J.EST.2020.101329.
[37] T. Kim, W. Choi, H.C. Shin, J.Y. Choi, J.M. Kim, M.S. Park, W.S. Yoon, Applications of voltammetry in lithium ion battery research, J. Electrochem. Sci. Technol. 11 (2020) 14–25, https://doi.org/10.33961/jecst.2019.00619.
[38] J.L. Lorie Lopez, P.J. Grandinetti, A.C. Co, Enhancing the real-time detection of phase changes in lithium–graphite intercalated compounds through derivative operando (dOp) NMR cyclic voltammetry, J. Mater. Chem. A. 6 (2017) 231–243, https://doi.org/10.1039/C7TA07521A.
[39] A. Dmitriev, Nanoplasmonic Sensors, 2012.
[40] T.S. Pathan, M. Rashid, M. Walker, W.D. Widanage, E. Kendrick, Active formation of Li-ion batteries and its effect on cycle life, J. Phys. Energy 1 (2019), https://doi.org/10.1088/2515-7655/ab2e92.
[41] I. Landa-Medrano, A. Eguia-Barrio, S. Sananes-Israel, S. Lijó-Pando, I. Boyano, F. Alcaide, I. Urdampilleta, I. de Meatza, In situ analysis of NMC|graphite Li-ion batteries by means of complementary electrochemical methods, J. Electrochem. Soc. 167 (2020), 090528, https://doi.org/10.1149/1945-7111/ab8b99.
[42] R. Jung, M. Metzger, F. Maglia, C. Stinner, H.A. Gasteiger, Oxygen release and its effect on the cycling stability of LiNi x Mn y Co z O 2 (NMC) cathode materials for Li-ion batteries, J. Electrochem. Soc. 164 (2017) A1361–A1377, https://doi.org/10.1149/2.0021707jes.
[43] K. Fröhlich, I. Abrahams, M. Jahn, Determining phase transitions of layered oxides via electrochemical and crystallographic analysis, Sci. Technol. Adv. Mater. 21 (2020) 653–660, https://doi.org/10.1080/14686996.2020.1814116.
[44] H.J. Noh, S. Youn, C.S. Yoon, Y.K. Sun, Comparison of the structural and electrochemical properties of layered Li[NixCoyMnz]O2 (x = 1/3, 0.5, 0.6, 0.7, 0.8 and 0.85) cathode material for lithium-ion batteries, J. Power Sources 233 (2013) 121–130, https://doi.org/10.1016/j.jpowsour.2013.01.063.
[45] K.M. Shaju, G.V. Subba Rao, B.V.R. Chowdari, Performance of layered Li(Ni1/3Co1/3Mn1/3)O2 as cathode for Li-ion batteries, Electrochim. Acta 48 (2002) 145–151, https://doi.org/10.1016/S0013-4686(02)00593-5.
[46] X.H. Shi, Y.P. Wang, X. Cao, S. Wu, Z. Hou, Z. Zhu, Charge compensation mechanisms and oxygen vacancy formations in LiNi1/3Co1/3Mn1/3O2: first-principles calculations, ACS Omega. 7 (2022) 14875, https://doi.org/10.1021/ACSOMEGA.2C00375.
[47] A.J. Louli, L.D. Ellis, J.R. Dahn, Operando pressure measurements reveal solid electrolyte interphase growth to rank Li-ion cell performance, Joule. 3 (2019) 745–761, https://doi.org/10.1016/j.joule.2018.12.009.
[48] M. Nascimento, S. Novais, C. Leitão, M.F. Domingues, N. Alberto, P. Antunes, J. L. Pinto, Lithium batteries temperature and strain fiber monitoring, in: 24th Int. Conf. Opt. Fibre Sensors, SPIE, 2015, p. 96347V, https://doi.org/10.1117/12.2195218.
[49] Y. Yu, E. Vergori, F. Maddar, Y. Guo, D. Greenwood, J. Marco, Real-time monitoring of internal structural deformation and thermal events in lithium-ion cell via embedded distributed optical fibre, J. Power Sources 521 (2022), 230957, https://doi.org/10.1016/j.jpowsour.2021.230957.
[50] J.R. Dahn, Phase diagram of LixC6, Phys. Rev. B 44 (1991) 9170–9177, https://doi.org/10.1103/PhysRevB.44.9170.
[51] S.C. Yin, Y.H. Rho, I. Swainson, L.F. Nazar, X-ray/neutron diffraction and electrochemical studies of lithium De/Re-intercalation in Li1-xCo1/3Ni1/3Mn 1/3O2 (x = 0 → 1), Chem. Mater. 18 (2006) 1901–1910, https://doi.org/10.1021/cm0511769.